

## Thermodynamic Bias in the Multimodel Mean Boreal Summer Monsoon\*

WILLIAM R. BOOS AND JOHN V. HURLEY

*Department of Geology and Geophysics, Yale University, New Haven, Connecticut*

(Manuscript received 26 July 2012, in final form 26 September 2012)

### ABSTRACT

Here it is shown that almost all models participating in the Coupled Model Intercomparison Project (CMIP) exhibit a common bias in the thermodynamic structure of boreal summer monsoons. The strongest bias lies over South Asia, where the upper-tropospheric temperature maximum is too weak, is shifted southeast of its observed location, and does not extend as far west over Africa as it does in observations. Simulated Asian maxima of surface air moist static energy are also too weak and are located over coastal oceans rather than in their observed continental position. The spatial structure of this bias suggests that it is caused by an overly smoothed representation of topography west of the Tibetan Plateau, which allows dry air from the deserts of western Asia to penetrate the monsoon thermal maximum, suppressing moist convection and cooling the upper troposphere. In a climate model with a decent representation of the thermodynamic state of the Asian monsoon, the qualitative characteristics of this bias can be recreated by truncating topography just west of the Tibetan Plateau. This relatively minor topographic modification also produces a negative anomaly of Indian precipitation of similar sign and amplitude to the CMIP continental Indian monsoon precipitation bias. Furthermore, in simulations of next-century climate warming, this topographic modification reduces the amplitude of the increase in Indian monsoon precipitation. These results confirm the importance of topography west of the Tibetan Plateau for South Asian climate and illustrate the need for careful assessments of the thermodynamic state of model monsoons.

### 1. Introduction

Monsoons are thermally direct, continental-scale circulations that supply water to billions of people, so simulations of present and future monsoons are widely studied. Because precipitation is a variable of great societal interest, it might seem logical to assess monsoon simulations by their skill in reproducing this variable, but precipitation fields are difficult to compare as they have numerous maxima and large variance on relatively short spatial scales. Most climate models poorly simulate the location and intensity of observed precipitation maxima in the South Asian and African monsoons even though they reasonably represent the regional-mean precipitation amount and its annual cycle in those areas

(Wang et al. 2004; Annamalai et al. 2007; Christensen et al. 2007). The implication of such bias for model sensitivity to a climate forcing is unclear.

When simulating a thermally direct circulation, one might alternatively ask whether the observed thermodynamic structure of a fluid is reproduced. Regardless of how well a model simulates vertical motion in thermally direct flow, which, in the tropics, is nearly equivalent to simulating precipitation, one might doubt its realism if it has a large temperature bias. A thermodynamic assessment may be especially appropriate for monsoons, most of which exhibit an observed seasonal-mean structure consistent with a convective quasi-equilibrium (QE) framework (Nie et al. 2010), which has been used in theoretical studies of monsoon dynamics (Chou et al. 2001; Neelin 2007). In such a framework, cumulus convection vertically couples temperature within the convecting layer to the moist static energy of air below cloud base  $h_b$ , so that those two quantities covary (Arakawa and Schubert 1974; Emanuel et al. 1994). But deep convection in monsoons tends to occur in a narrow, large-scale ascent zone near the free-tropospheric temperature maximum; in the subsiding branch of the circulation, moist convection is suppressed and  $h_b$  is decoupled from

---

\* Supplemental information related to this paper is available at the Journal's Online website: <http://dx.doi.org/10.1175/JCLI-D-12-00493.s1>.

---

Corresponding author address: William R. Boos, Department of Geology and Geophysics, Yale University, P.O. Box 208109, New Haven, CT 06520-8109.  
E-mail: billboos@alum.mit.edu

free-tropospheric temperature. Maxima of  $h_b$  and free-tropospheric temperature are thus coincident for monsoons in a QE framework, and the locations of these maxima mark the poleward edge of the ascent branch of the thermally direct monsoon circulation (e.g., Lindzen and Hou 1988; Emanuel 1995; Privé and Plumb 2007a).

Here, we assess how well two suites of climate models reproduce the observed thermodynamic structures of monsoons. Because we desire a diagnostic that can be used with available climate model output, we use surface air moist static energy as the measure of  $h_b$  and temperature averaged between 200 and 400 hPa in the upper troposphere  $T_u$  as the measure of temperature within the convecting layer. These quantities exhibit highly similar distributions to the moist entropy variables used in previous observational analyses (Boos and Emanuel 2009; Nie et al. 2010; Boos and Kuang 2010).

## 2. Data, models, and methods

This study uses model output from phases 3 and 5 of the Coupled Model Intercomparison Project (CMIP), established by the World Climate Research Programme's Working Group on Coupled Modeling. We calculated  $h_b$  at a standard reference height 2 m above the land or ocean surface and expressed it in temperature units by dividing by the specific heat of dry air at constant pressure ( $1005.7 \text{ J kg}^{-1} \text{ K}^{-1}$ ). We calculated  $T_u$  as a mass-weighted vertical average from 200 to 400 hPa. All analyses were performed using monthly data averaged for 1979–99 from the twentieth-century integrations that employed both natural and anthropogenic forcings: the “20c3m” and “historical” experiments for CMIP3 and CMIP5, respectively. Locations of thermal maxima seem insensitive to the averaging period. The 15 CMIP3 and 13 CMIP5 models having the requisite data for this analysis are listed in Table 1, and we use only one ensemble member from each model. Surface winds were not available for three CMIP5 models (CanESM2, CCSM4.0, and FGOALS-g2), so the surface wind bias shown is for the remaining models.

Model results were compared with averages for the same time period from the latest European Centre for Medium-Range Weather Forecasts (ECMWF) Interim Re-Analysis (ERA-Interim; hereafter, ERA-Int) (Dee et al. 2011). ERA-Int uses a spectral T255 atmospheric model with 60 vertical levels, and gridded output is available at a horizontal resolution of  $0.7^\circ$  latitude  $\times$   $0.7^\circ$  longitude. Although reanalysis products are not directly constrained by data in all times and locations, previous analysis of radiosonde subcloud entropy and satellite-derived upper-tropospheric temperatures produced a consistent climatology for South Asia (Boos and

Kuang 2010). All model results were interpolated onto the ERA-Int grid before computing averages and differences. All testing of statistical significance was performed using two-tailed Student's *t* tests with a 5% significance level.

Model surface elevations were compared with the 2-minute Gridded Global Relief Data (ETOPO2v2) dataset, which has a horizontal resolution of 2 arc minutes and was obtained from the National Geophysical Data Center (NGDC), National Oceanic and Atmospheric Administration (NOAA), U.S. Department of Commerce. Model precipitation was compared with the Global Precipitation Climatology Project (GPCP) (Adler et al. 2003) for 1979–99.

The Community Earth System Model (CESM), version 1.0.4, of the National Center for Atmospheric Research (NCAR) was integrated with standard topography and also with topography in the region  $29^\circ\text{--}40^\circ\text{N}$ ,  $62^\circ\text{--}71^\circ\text{E}$  that is higher than 1 km reduced to a height of 1 km (this truncates the Hindu Kush range just west of the Tibetan Plateau). All integrations were performed at  $0.9^\circ \times 1.25^\circ$  horizontal resolution with 26 vertical levels with fully active and coupled atmosphere, ocean, sea ice, and land models. One set of integrations was performed using present-day forcings and initial conditions (the CESM B\_2000 component set), with results averaged over the last 20 years of a 21-yr run, using standard topography and then using the aforementioned truncated topography. A third integration was performed by relaxing specific humidities southeast of the Hindu Kush (between  $25^\circ$  and  $37^\circ\text{N}$  and between  $60^\circ$  and  $76^\circ\text{E}$ ) to zero over a time scale of 6 days in a model with standard topography. This violates global conservation of energy and water but was done only as an idealized process study; we expect that prescribing a spatially diffuse, compensating moisture source would not change the response qualitatively. Finally, another set of CESM integrations was performed for 100 years with forcings from representative concentration pathway (RCP) 8.5, the most extreme CMIP5 scenario for greenhouse gas increases (CESM component set B\_RCP8.5\_CN). A four-member ensemble was integrated using standard topography and another using the modified topography, with initial conditions drawn from four different times in NCAR's preindustrial control run. Results shown for the next-century simulations are ensemble means.

## 3. Results and discussion

### a. CMIP analyses

The mean of all CMIP5 models exhibits a boreal summer maximum of  $h_b$  over South Asia that is too weak when compared with ERA-Int and is located over coastal

TABLE 1. CMIP models used in this study.

Archive	Modeling center/group	Model name	Model name expansion
CMIP3	Canadian Centre for Climate Modelling and Analysis Canadian Centre for Climate Modelling and Analysis	CGCM3.1(T47) CGCM3.1(T63)	Coupled Global Climate Model, version 3.1 (T47 spectral resolution) Coupled Global Climate Model, version 3.1 (T63 spectral resolution)
Météo-France/Centre National de Recherches Météorologiques (CNRM) Commonwealth Scientific and Industrial Research Organisation (CSIRO) Atmospheric Research		CNRM-CM3 CSIRO Mk3.0	CNRM Coupled Global Climate Model, version 3 CSIRO Mark 3.0
CSIRO Atmospheric Research		CSIRO Mk3.5 GISS-AOM	CSIRO Mark 3.5 GISS Atmosphere–Ocean Model
National Aeronautics and Space Administration (NASA) Goddard Institute for Space Studies (GISS)		GISS-EH GISS-ER FGOALS-g1.0	GISS Model E Coupled with HYCOM Ocean Model GISS Model E Coupled with Russell Ocean Model Flexible Global Ocean–Atmosphere–Land System Model, gridpoint version 1.0
NASA Goddard Institute for Space Studies		INM-CM3.0 IPSL-CM4 MIROC3.2 (hires)	INM Coupled Model, version 3.0 IPSL Coupled Model, version 4 Model for Interdisciplinary Research on Climate, version 3.2 (high-resolution)
NASA Goddard Institute for Space Studies		MIROC3.2 (medres)	Model for Interdisciplinary Research on Climate, version 3.2 (medium-resolution)
State Key Laboratory of Numerical Modeling for Atmospheric Sciences and Geophysical Fluid Dynamics (LASG)/Institute of Atmospheric Physics Institute of Numerical Mathematics (INM)		CCSM3.0 BCCR-BCM2.0 CSIRO Mk3.6.0 CanESM2 GISS-E2-R HadGEM2-ES	Community Climate System Model, version 3.0 BCCR Bergen Climate Model, version 2.0 CSIRO Mark 3.6.0 Second-generation Canadian Earth System Model GISS Model E2 Coupled with Russell Ocean Model Hadley Centre Global Environmental Model, version 2 (Earth System)
L'Institut Pierre-Simon Laplace (IPSL) Center for Climate System Research (University of Tokyo), National Institute for Environmental Studies, Frontier Research Center for Global Change, and Japan Agency for Marine-Earth Science and Technology (JAMSTEC)		IPSL-CM5A-LR MIROC4h	IPSL Coupled Model, version 5A (low resolution) Model for Interdisciplinary Research on Climate, version 4 (high-resolution)
Center for Climate System Research (University of Tokyo), National Institute for Environmental Studies, Frontier Research Center for Global Change, and JAMSTEC		MIROC5	Model for Interdisciplinary Research on Climate, version 5
National Center for Atmospheric Research Bjerknes Centre for Climate Research (BCCR)		MRI-CGCM3 CNRM-CM5	MRI Coupled General Circulation Model, version 3 CNRM Coupled Global Climate Model, version 5
CSIRO in collaboration with Queensland Climate Change Centre of Excellence Canadian Centre for Climate Modeling and Analysis		CCSM4.0 GFDL-ESM2G FGOALS-g2	Community Climate System Model, version 4.0 GFDL Earth System Model with GOLD ocean component (2G) Flexible Global Ocean–Atmosphere–Land System Model, gridpoint version 2
NASA Goddard Institute for Space Studies Met Office Hadley Centre		INM-CM4.0	INM Coupled Model, version 4.0
L'Institut Pierre-Simon Laplace Center for Climate System Research (University of Tokyo), National Institute for Environmental Studies, Frontier Research Center for Global Change, and Japan Agency for Marine-Earth Science and Technology (JAMSTEC)			
Centre National de Recherches Météorologiques (CNRM)/Centre Européen de Recherche et Formation Avancées en Calcul Scientifique			
National Center for Atmospheric Research NOAA Geophysical Fluid Dynamics Laboratory (GFDL) LASG/Institute of Atmospheric Physics, Chinese Academy of Sciences, and Center for Earth System Science (Tsinghua University)			
Institute of Numerical Mathematics (INM)			

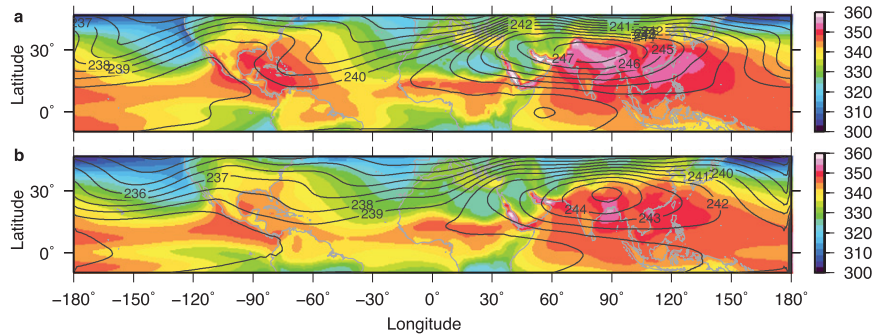


FIG. 1. July mean (1979–99) surface air moist static energy  $h_b$  (shading; K) and upper-tropospheric temperature  $T_u$  (contours; K) for (a) ERA-Int and (b) the CMIP5 multimodel mean.

oceans rather than in its observed continental position over northwest India and Pakistan (Fig. 1). The CMIP5 global maximum of  $T_u$  is similarly positioned south and east of its observed location over northern India and is weaker than observed in both amplitude and zonal width, especially in its westward extension over Africa. The thermal ridge associated with the North American monsoon is weaker in CMIP5 than in ERA-Int, and  $h_b$  over the Caribbean Sea and just west of Mexico is too low. Although maxima in a multimodel mean may be weaker than in any single model simply because of scatter in the location of individual model peaks, the global  $T_u$  maxima in nearly all models are shifted south and/or east of the observed peak (green triangles in Fig. 2) and are weaker than observed. Individual model

distributions of  $h_b$  and  $T_u$  (shown in the supplemental material) typically deviate from observations much more than the multimodel mean, although three or four of the 13 models in CMIP5 do have global maxima of both  $h_b$  and  $T_u$  located over northern India. Note that the Red Sea and Persian Gulf stand out in the high-resolution ERA-Int dataset as global  $h_b$  maxima, and the  $h_b$  bias over these bodies of water is weaker and less statistically significant in CMIP5 than in CMIP3, likely because of higher model resolution (Fig. 2). The influence of the Persian Gulf and Red Sea on the Asian monsoon is unknown, although any influence may be reduced by horizontal mixing with nearby low- $h_b$  air.

When plotted as an anomaly relative to observations, the weakening and southeastward shift of model

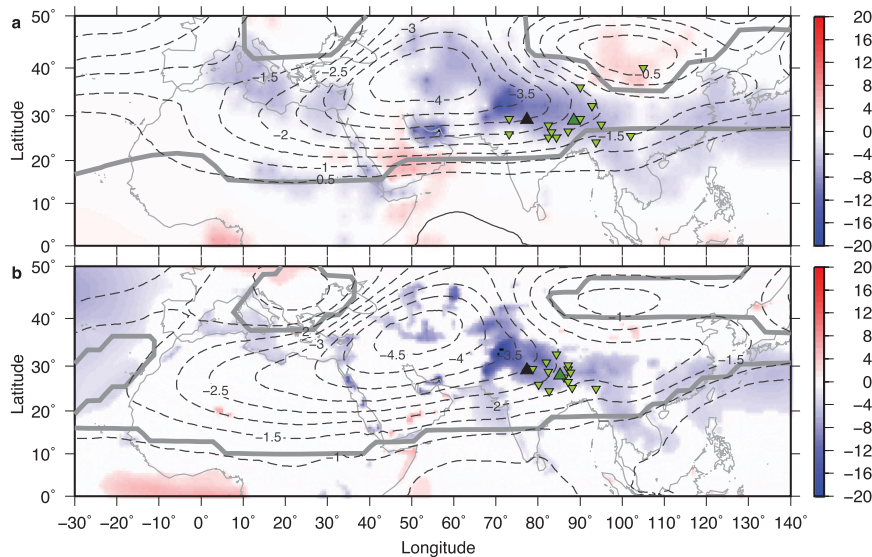


FIG. 2. (a) CMIP3 and (b) CMIP5 July mean (1979–99) biases, relative to ERA-Int, in  $h_b$  (shading; K) and  $T_u$  (contours; K). A thick gray line surrounds regions with statistically significant  $T_u$  anomalies, and only statistically significant  $h_b$  anomalies are plotted. Location of maximum  $T_u$  is shown by inverted green triangles for each model, by large green triangles for the multimodel mean, and by black triangles for ERA-Int. Only 14 inverted triangles are visible in (a) because two of those symbols overlap.

thermodynamic maxima appear as a negative anomaly of  $h_b$  with peak amplitude adjacent to the mountains of northwest India and Pakistan (Figs. 2 and 3b). This negative  $h_b$  anomaly is caused almost entirely by a bias in specific humidity (not shown). A cold  $T_u$  anomaly extends westward from this  $h_b$  anomaly across the Arabian Peninsula and northern Africa. Similar biases are seen in the CMIP3 and CMIP5 ensembles, indicating little improvement in the mean thermodynamic structure of the latest generation of models (though the CMIP5  $T_u$  maxima are more clustered and have a multimodel mean location closer to that observed). Except for the positive anomaly of  $h_b$  over the Gulf of Guinea, which is consistent with the known CMIP warm SST bias in that region (Christensen et al. 2007), any oceanic bias in  $h_b$  is much weaker than the continental bias over northwest India and Pakistan. Since SST is expected to exert a strong local control on  $h_b$ , there is thus no obvious indication that the continental  $h_b$  bias results directly from an SST bias. Furthermore, the  $h_b$  and  $T_u$  bias in eight atmospheric GCMs forced by SST and archived as part of the CMIP5 project had peak negative anomalies of similar amplitude and location (not shown). Note that the continental  $h_b$  bias over South Asia has higher amplitude than the comparatively much-studied Gulf of Guinea bias.

We hypothesize that the negative CMIP  $h_b$  anomaly results from advection of low- $h_b$  air across smoothed model topography, with moist convection communicating this anomaly to the upper troposphere, where it spreads zonally across the Middle East and Africa via Rossby wave activity. Previous studies have suggested that topography may create a strong monsoon by preventing extratropical air with low moist static energy from mixing with the monsoon thermal maximum (Boos and Kuang 2010; Privé and Plumb 2007b), with topography west of the Tibetan Plateau playing a particularly important role (Chakraborty et al. 2006). To avoid the introduction of grid-scale noise, topography in climate models is often smoothed to have minimum length scales larger than that of the model numerical grid (Rivest et al. 1994; Rutt et al. 2006). Some models modify surface drag to represent unresolved orographic blocking (Webster et al. 2003; Neale et al. 2010), but it is unclear which models use such blocking schemes and whether they adequately account for the effects of unrepresented topographic variance. Topographic smoothing in models would presumably introduce the strongest bias in regions of high topographic variance, such as west of the Tibetan Plateau.

Maximum topographic heights adjacent to the observed  $h_b$  maximum over northern India are indeed underrepresented by at least 1 km in even the highest

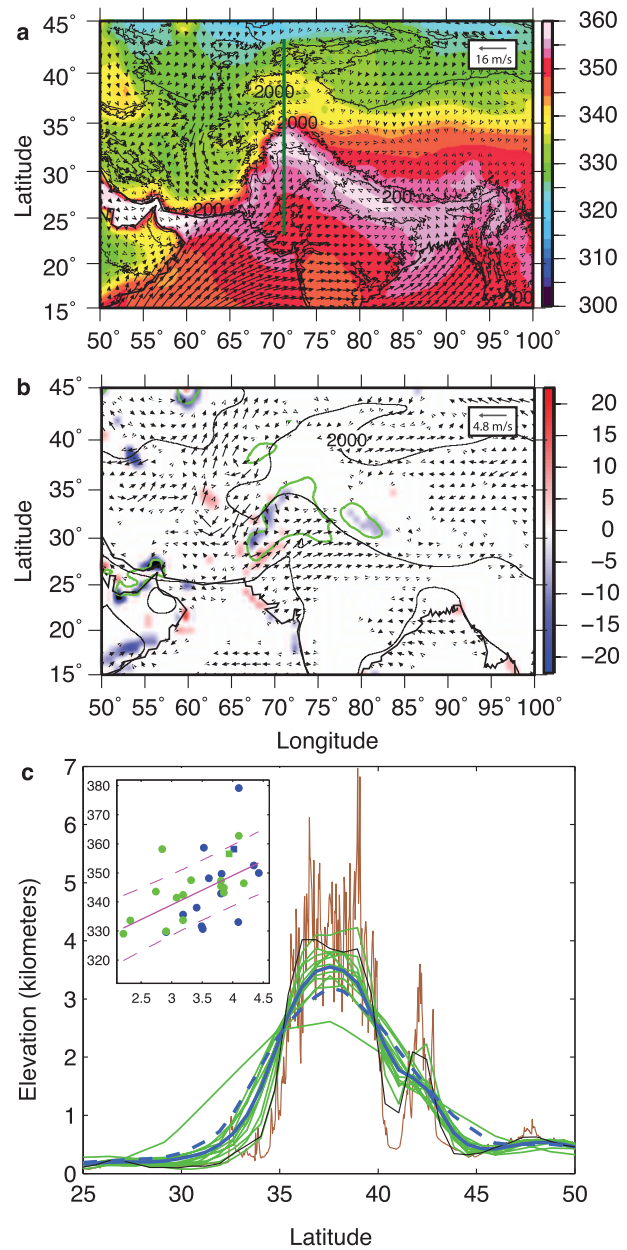


FIG. 3. (a) ERA-Int July 10-m wind (vectors),  $h_b$  (shading; K), and observed topography (black contours; m). (b) CMIP5 July biases in 10-m wind (vectors) and horizontal  $h_b$  advection by time-mean winds (shading; K day $^{-1}$ ). Black contours show multimodel mean topography (m), green contours represent a CMIP5  $h_b$  bias of  $-10\text{ K}$ , and only statistically significant biases in winds and advection are shown. (c) Topography along 72°E [green line in (a)] for observations (brown line), CMIP5 and CMIP3 multimodel means (solid and dashed thick blue lines, respectively), individual CMIP5 models (green lines), and ERA-Int (thin black line). Inset shows maximum  $h_b$  over northwestern India, 31°–34°N, 68°–74°E (vertical axis) plotted against maximum topographic height (km) along 72°E for CMIP3 (green dots) and CMIP5 (blue dots). Magenta lines in inset show a best linear fit and its uncertainty.

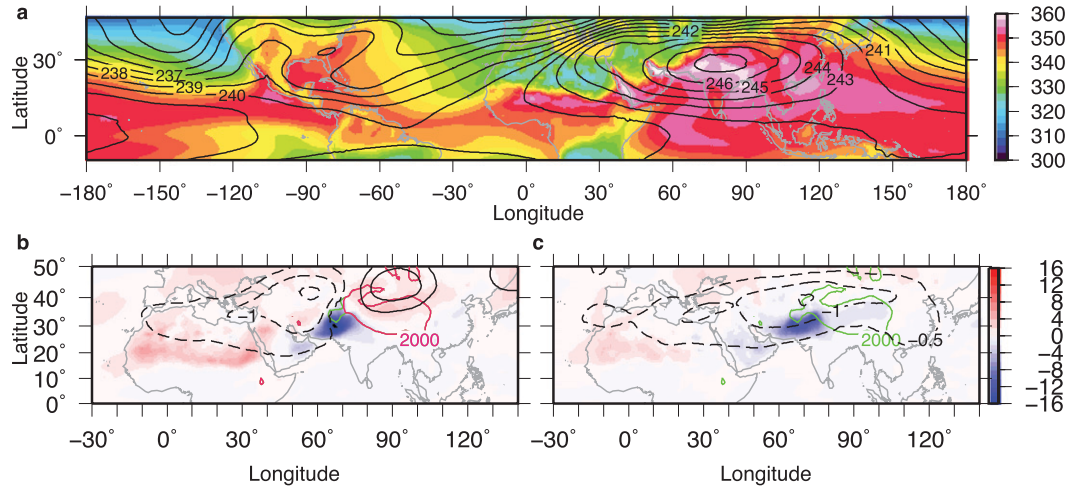


FIG. 4. (a) As in Fig. 1, but for CESM with standard topography. (b) As in Fig. 2, but for the anomaly, relative to the control run, in the CESM run with a truncated Hindu Kush range. Negative  $T_u$  contours are dashed and positive are solid, with a contour interval of 0.5 K and the zero line not shown. The 2-km topographic contour is green and pink in the runs with standard and truncated topography, respectively. (c) The anomaly created by imposing a moisture sink over northwestern India in the model with standard topography.

resolution CMIP5 models (Fig. 3c).<sup>1</sup> The observed climatology of surface wind shows strong southward flow west of the Tibetan Plateau that advects low- $h_b$  air from the extratropics into the desert regions of southwestern Asia (Fig. 3a). Much of this flow is ageostrophic, down the strong meridional pressure gradient into the intense climatological heat low in that region (Ramage 1966; Bollasina and Nigam 2011), but is diverted around the topography of Afghanistan's Hindu Kush mountains (near 35°N, 67°E). The CMIP5 models produce anomalous southward flow over the smoothed Hindu Kush and anomalous northward flow to their west, indicating an eastward shift in the observed southward flow into the desert heat low. The bias in 700-hPa wind (not shown) is similar to this surface wind bias. We computed the time tendency of  $h_b$  from horizontal advection by the time-mean flow, and the CMIP5 models have a negative bias, relative to ERA-Int, in the region where the  $h_b$  anomaly is most strongly negative (Fig. 3b, near 32°N, 68°E). There are other extrema in the advective bias that do not correspond to large  $h_b$  anomalies, but this is not surprising given that there could be an influence from other advective terms (e.g., transient eddies) or from source terms. Unfortunately, the CMIP5 archive does not contain the daily, vertically resolved data needed to

compute the full moist static energy budget for the ensemble of models analyzed here. Nevertheless, it is notable that the bias in horizontal advection by time-mean winds is strong enough to reduce the monsoon  $h_b$  maximum to extratropical values within a few days.

These biases in low-level wind,  $h_b$ , and horizontal  $h_b$  advection are consistent with the hypothesis that highly smoothed model topography allows ventilation of the monsoon thermal maximum by dry extratropical air. This confirms the previous finding that topography west of the Tibetan Plateau creates a strong monsoon by suppressing horizontal advection of low- $h_b$  air into the monsoon thermal maximum (Chakraborty et al. 2006); here we employ that idea to understand one effect of the topographic smoothing used in climate models. Finally, we note that there is a positive relationship (correlation coefficient 0.50) between the maximum topographic height along 72°E in the models and the maximum value of  $h_b$  over northwestern India within 31°–34°N, 68°–74°E (Fig. 3c, inset). Considerable scatter is expected in this relationship because of individual model bias in surface albedo, mean state winds, and other controls on  $h_b$ .

#### b. Model integrations

A more conclusive test of our hypothesis involves reproducing the CMIP bias by altering topography in a model with a realistic thermodynamic climatology. NCAR produced one of the few models with thermal maxima located near the observed location for the model versions used in CMIP3 and CMIP5 and for a more recent version (CESM) integrated for this study (cf. Figs. 4a and 1a). This CESM version does not use a subgrid-scale

<sup>1</sup> The longitude of 72°E was chosen for the profile in Fig. 3c because it has a topographic variance low enough to allow a plot of 13 model profiles plus observations to be readable. This longitude is slightly east of the region in which we truncate topography in the model integrations presented in section 3b but illustrates a similar model underestimate of peak topographic height.

orographic blocking scheme, nor does it have horizontal resolution finer than that of many other CMIP models. It does, however, have a lower broadband surface albedo over India than that estimated from ERA-Int (not shown), suggesting that errors in one regional energy source may compensate for opposite errors in another. Although CESM is thus not a perfect model for our purpose, it can provide a useful framework for examining the effect of reductions in topographic heights. Limiting the Hindu Kush mountains to a maximum height of 1 km in CESM recreated a bias similar to that seen in the CMIP models (cf. Figs. 4b and 2). A negative  $h_b$  anomaly occurs southeast of the truncated orography, and a cold  $T_u$  anomaly stretches across northern Africa west of the modified orography. The  $T_u$  anomaly is about one-third the amplitude of that seen in the CMIP multimodel mean but has a similar spatial structure.

The cold  $T_u$  anomaly extending across northern Africa can also be recreated using standard model topography with a moisture sink imposed southeast of the Hindu Kush, intended to crudely represent the effect of dry air advection across that topography (Fig. 4c). The negative  $h_b$  anomaly local to the moisture sink occurs by construction, but the accompanying cold  $T_u$  anomaly is associated with weakened deep convection over northern India and presumably spreads westward via Rossby waves (Gill 1980; Rodwell and Hoskins 1996). The linear Rossby gyre induced by negative convective heating over South Asia consists of low-level southeasterlies over northern Africa, which would advect high- $h_b$  air meridionally from the Sahel into the Sahara and zonally from the Arabian and Red Seas into the Sahara. The surface and 700-hPa wind do have a southeasterly bias that roughly follows contours of the  $T_u$  anomalies shown in Fig. 4, as expected for a first-baroclinic, geostrophic response. This might explain the positive  $h_b$  anomaly seen in northern Africa in our perturbed CESM integrations. A similar positive  $h_b$  bias was seen over Africa in some CMIP models (not shown) but was not statistically significant in the multimodel mean (Fig. 2).

The dry, linear response to a reduction of topography in mean westerlies does include a cold anomaly immediately upstream of the topographic depression (e.g., Held et al. 2002), but we estimate that this dry response is of much lower magnitude and zonal extent than the  $T_u$  anomalies seen in our moist models. We integrated the dry dynamical core of CESM using the idealized physics scheme of Held and Suarez (1994), first with standard topography and then with our truncated topography. In this dry model, the topographic truncation produced a  $T_u$  anomaly having one-fourth the magnitude and a different horizontal structure than seen in the moist model (not shown). Furthermore, the standard Held and

Suarez (1994) configuration has a weaker static stability than that of the observed tropical atmosphere and should overestimate the vertical extent of the response (Johnson 1977). Repeating the dry model runs with a higher basic state static stability indeed produced an even weaker  $T_u$  response. The dry model also produced a low-level response highly similar to that seen in the model of Bollasina and Nigam (2011), which was linearized about the observed zonal mean boreal summer state, when we integrated our model with their topographic forcings (not shown). This is all consistent with the dry dynamical effect of our topographic truncation on  $T_u$  being weak relative to the anomalies seen in the moist CESM.

A practical question is whether this thermodynamic bias influences simulated rainfall. Relative to the model with standard topography, the model with a truncated Hindu Kush produces less precipitation over India in its simulation of modern climate (Fig. 5b).<sup>2</sup> This bias is similar in sign and amplitude to the CMIP5 multimodel mean bias in continental Indian precipitation (Fig. 5a) and is consistent with intrusions of low- $h_b$  air into India, rendering the troposphere more convectively stable. It is also consistent with a simple conceptual model of the monsoon as a thermally direct, meridional overturning circulation: reducing the amplitude of the monsoon thermal maximum and shifting this maximum toward the equator causes a weakening and equatorward shift of the precipitating ascent branch of the overturning circulation (Lindzen and Hou 1988; Emanuel 1995; Privé and Plumb 2007a).

To gauge the effect of the topographic perturbation on simulated next-century rainfall, we constructed an index of Indian monsoon precipitation by averaging precipitation over land regions within  $5^{\circ}$ – $33^{\circ}$ N,  $70^{\circ}$ – $89^{\circ}$ E (box in Fig. 5b). The CESM configuration with truncated topography predicts a next-century increase in the summer mean (May–August) value of this precipitation index that is about 40% weaker than in the model with standard orography, with this difference being significant by a Student's  $t$  test at the 5% level. The model with truncated topography simulates a next-century delay in the seasonal onset of monsoon rainfall and an associated decrease in June precipitation over the next century, in contrast with the control model, which exhibits a net increase in June precipitation (Fig. 5c). The gradient in  $h_b$  across the Hindu Kush becomes stronger in the next

<sup>2</sup> Although plots of  $h_b$  and  $T_u$  were shown for July, precipitation is averaged for May–September because this is more conventional and because changes in the onset date of monsoon precipitation can have a large effect on total summer precipitation. Nevertheless, the July distributions were qualitatively similar (not shown).

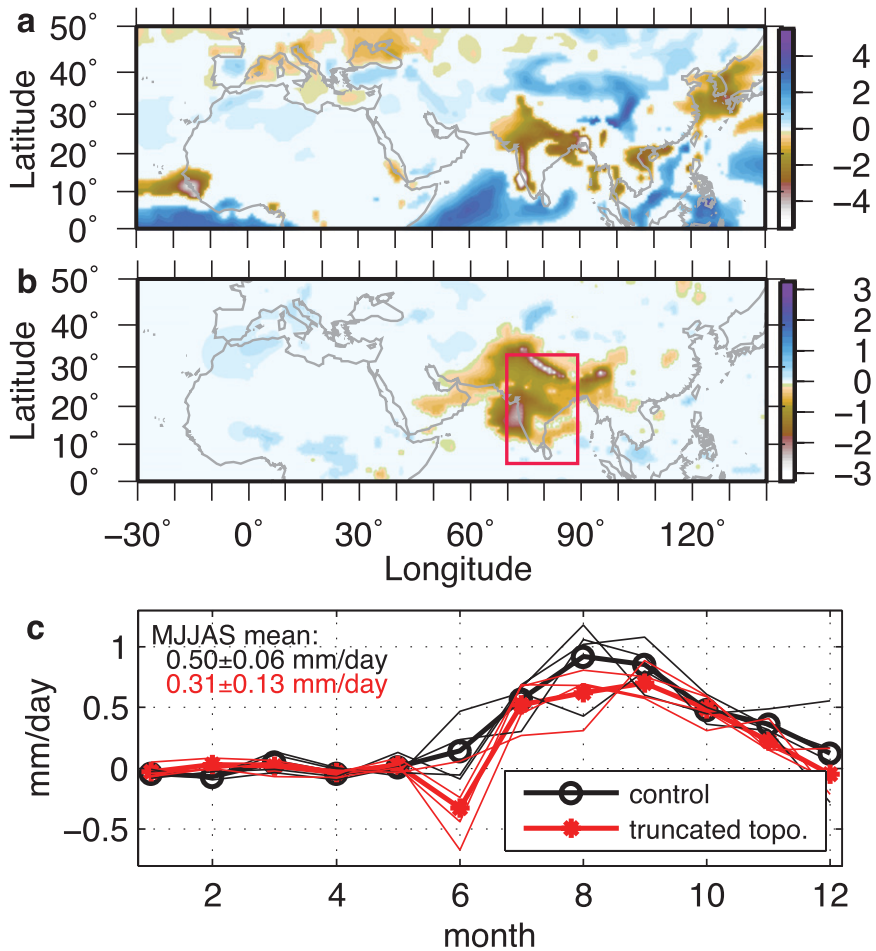


FIG. 5. (a) CMIP5 bias, relative to observations (GPCP) in 1979–99 May–September precipitation ( $\text{mm d}^{-1}$ ). (b) Anomaly in the May–September precipitation ( $\text{mm day}^{-1}$ ) in the present climate (2005–24), relative to the control run, in the CESM model with a truncated Hindu Kush range. Red box surrounds the region within which land precipitation was horizontally averaged to obtain the index plotted in (c). (c) Annual cycle of the next-century change in Indian precipitation index (the period 2085–2104 minus the period 2005–24) for the control model (black) and the model with truncated Hindu Kush (red). Thin lines represent individual ensemble members and thick lines the ensemble mean. The May–September mean change in the index is noted with its 95% confidence interval.

century (Fig. 6), consistent with the theory that predicts a warmer climate will have larger horizontal gradients of  $h_b$  between precipitating regions and neighboring dry regions (Chou and Neelin 2004; Neelin et al. 2003). Assuming no change in winds, horizontal advection of  $h_b$  across the Hindu Kush is thus expected to influence the South Asian monsoon even more strongly in a warmer climate, and this influence will be stronger in models with truncated topography. The next-century delay of onset in the model with truncated topography is consistent with the results of Chakraborty et al. (2006), who found that complete elimination of topography west of the Tibetan Plateau delayed Indian monsoon onset in simulations of present climate. However, our more minor topographic

truncation also reduced next-century precipitation by a similar amount in later summer (Fig. 5c).

In summary, this study presents a clear thermodynamic bias in climate models that persists from CMIP3 to CMIP5. It elucidates a likely cause of this bias, and shows that this bias can have practical importance for simulations and predictions of monsoon rainfall. Numerous issues merit further research, including fundamental questions concerning the interaction of moist convectively coupled flow with topography and interactions between monsoons and proximal deserts. Individual models likely have substantial thermodynamic bias because of factors other than topography (e.g., representations of surface albedo and moist convection), but the bias caused by

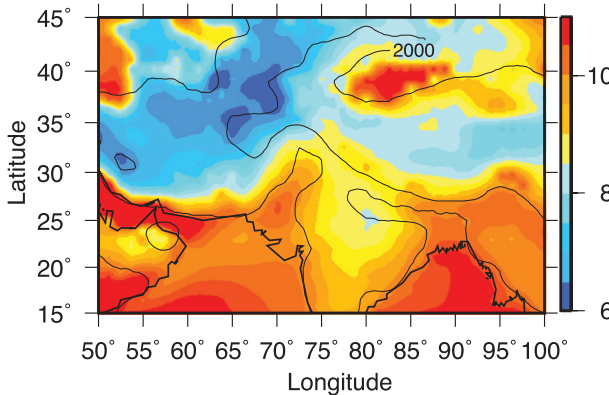


FIG. 6. Change in  $h_b$  (K) over the next century (2085–2104 minus 2005–24) in the CESM ensemble using standard topography. All values are statistically significant, and black contours represent model topography.

topographic smoothing stands out as one that does not average to zero in the multimodel mean. Importantly, models with thermodynamic climatologies that deviate greatly from observations may exhibit strongly biased sensitivities to thermal forcings such as changes in greenhouse gas concentrations.

**Acknowledgments.** Both authors acknowledge financial support from the Office of Naval Research Young Investigator Program Award N00014-11-1-0617 and from Yale University. We thank the climate modeling groups in Table 1 for making their model output available through CMIP. The U.S. Department of Energy's Program for Climate Model Diagnosis and Intercomparison supported CMIP software infrastructure in partnership with the Global Organization for Earth System Science Portals.

## REFERENCES

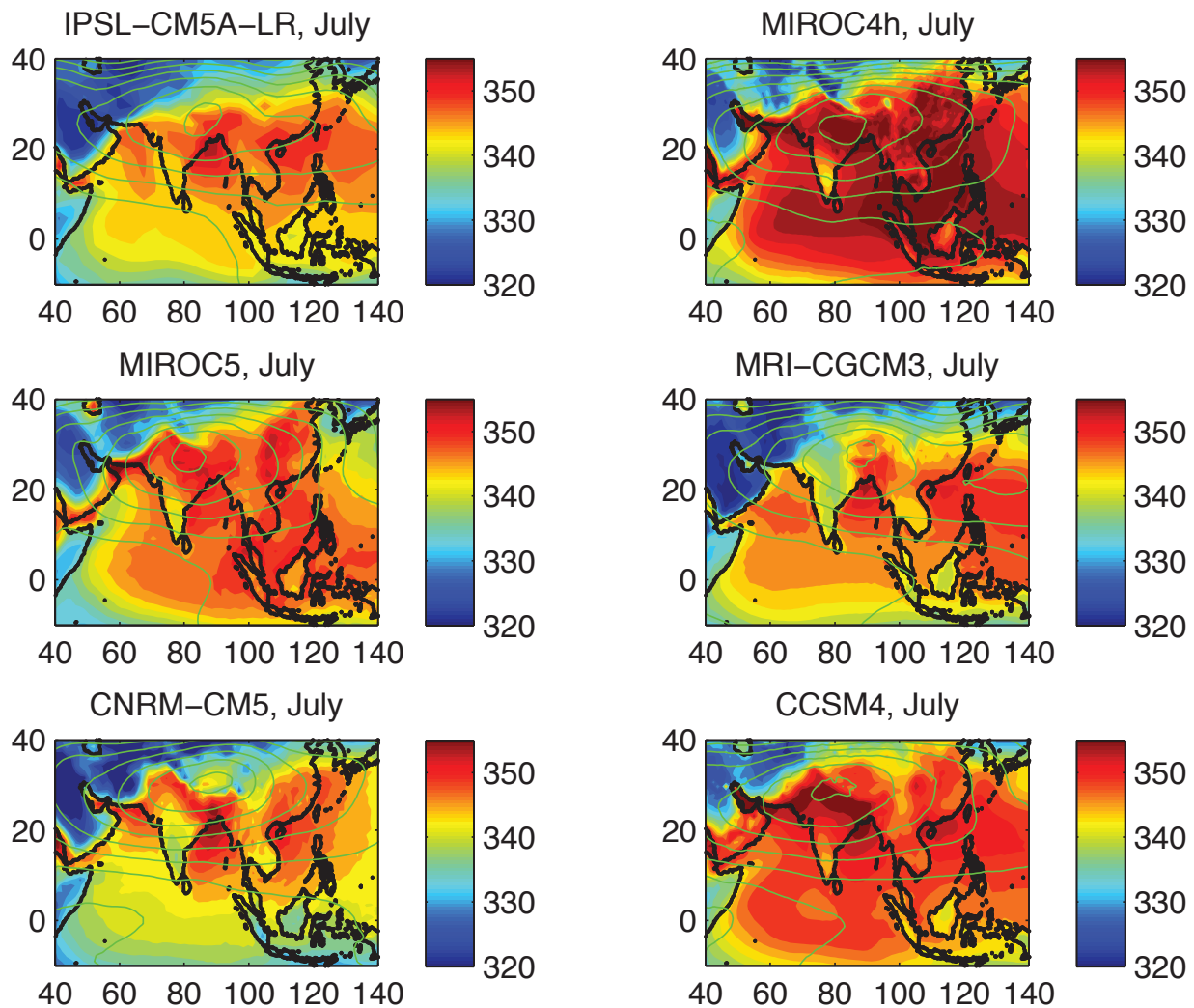
- Adler, R., and Coauthors, 2003: The Version-2 Global Precipitation Climatology Project (GPCP) monthly precipitation analysis (1979–present). *J. Hydrometeor.*, **4**, 1147–1167.
- Annamalai, H., K. Hamilton, and K. Sperber, 2007: The South Asian summer monsoon and its relationship with ENSO in the IPCC AR4 simulations. *J. Climate*, **20**, 1071–1092.
- Arakawa, A., and W. Schubert, 1974: Interaction of a cumulus cloud ensemble with the large-scale environment, Part I. *J. Atmos. Sci.*, **31**, 674–701.
- Ballasina, M., and S. Nigam, 2011: The summertime “heat” low over Pakistan/northwestern India: Evolution and origin. *Climate Dyn.*, **37**, 957–970.
- Boos, W. R., and K. A. Emanuel, 2009: Annual intensification of the Somali jet in a quasi-equilibrium framework: Observational composites. *Quart. J. Roy. Meteor. Soc.*, **135**, 319–335.
- , and Z. Kuang, 2010: Dominant control of the South Asian monsoon by orographic insulation versus plateau heating. *Nature*, **463**, 218–222.
- Chakraborty, A., R. Nanjundiah, and J. Srinivasan, 2006: Theoretical aspects of the onset of Indian summer monsoon from perturbed orography simulations in a GCM. *Ann. Geophys.*, **24**, 2075–2089.
- Chou, C., and J. Neelin, 2004: Mechanisms of global warming impacts on regional tropical precipitation. *J. Climate*, **17**, 2688–2701.
- , —, and H. Su, 2001: Ocean–atmosphere–land feedbacks in an idealized monsoon. *Quart. J. Roy. Meteor. Soc.*, **127**, 1869–1892.
- Christensen, J., and Coauthors, 2007: Regional climate projections. *Climate Change 2007: The Physical Science Basis*, S. Solomon et al., Eds., Cambridge University Press, 848–940.
- Dee, D., and Coauthors, 2011: The ERA-Interim reanalysis: Configuration and performance of the data assimilation system. *Quart. J. Roy. Meteor. Soc.*, **137**, 553–597.
- Emanuel, K. A., 1995: On thermally direct circulations in moist atmospheres. *J. Atmos. Sci.*, **52**, 1529–1536.
- , J. D. Neelin, and C. S. Bretherton, 1994: On large-scale circulations in convecting atmospheres. *Quart. J. Roy. Meteor. Soc.*, **120**, 1111–1143.
- Gill, A. E., 1980: Some simple solutions for heat-induced tropical circulation. *Quart. J. Roy. Meteor. Soc.*, **106**, 447–462.
- Held, I., and M. Suarez, 1994: A proposal for the intercomparison of the dynamical cores of atmospheric general circulation models. *Bull. Amer. Meteor. Soc.*, **75**, 1825–1830.
- , M. Ting, and H. Wang, 2002: Northern winter stationary waves: Theory and modeling. *J. Climate*, **15**, 2125–2144.
- Johnson, E., 1977: Stratified Taylor columns on a beta-plane. *Geophys. Astrophys. Fluid Dyn.*, **9**, 159–177.
- Lindzen, R. S., and A. Y. Hou, 1988: Hadley circulation for zonally averaged heating centered off the equator. *J. Atmos. Sci.*, **45**, 2416–2427.
- Neale, R., and Coauthors, 2010: Description of the NCAR Community Atmosphere Model (CAM 5.0). Tech. Rep., National Center for Atmospheric Research, Boulder, CO, 282 pp.
- Neelin, J., 2007: Moist dynamics of tropical convection zones in monsoons, teleconnections, and global warming. *The Global Circulation of the Atmosphere*, T. Schneider and A. H. Sobel, Eds., Princeton University Press, 267–301.
- , C. Chou, and H. Su, 2003: Tropical drought regions in global warming and El Niño teleconnections. *Geophys. Res. Lett.*, **30**, 2275, doi:10.1029/2003GL018625.
- Nie, J., W. Boos, and Z. Kuang, 2010: Observational evaluation of a convective quasi-equilibrium view of monsoons. *J. Climate*, **23**, 4416–4428.
- Privé, N. C., and R. A. Plumb, 2007a: Monsoon dynamics with interactive forcing. Part I: Axisymmetric studies. *J. Atmos. Sci.*, **64**, 1417–1430.
- , and —, 2007b: Monsoon dynamics with interactive forcing. Part II: Impact of eddies and asymmetric geometries. *J. Atmos. Sci.*, **64**, 1431–1442.
- Ramage, C., 1966: The summer atmospheric circulation over the Arabian Sea. *J. Atmos. Sci.*, **23**, 144–150.
- Rivest, C., A. Staniforth, and A. Robert, 1994: Spurious resonant response of semi-Lagrangian discretizations to orographic forcing: Diagnosis and solution. *Mon. Wea. Rev.*, **122**, 366–376.
- Rodwell, M., and B. Hoskins, 1996: Monsoons and the dynamics of deserts. *Quart. J. Roy. Meteor. Soc.*, **122**, 1385–1404.
- Rutt, I., J. Thuburn, and A. Staniforth, 2006: A variational method for orographic filtering in NWP and climate models. *Quart. J. Roy. Meteor. Soc.*, **132**, 1795–1813.
- Wang, B., I. Kang, and J. Lee, 2004: Ensemble simulations of Asian–Australian monsoon variability by 11 AGCMs. *J. Climate*, **17**, 803–818.
- Webster, S., A. Brown, D. Cameron, and C. Jones, 2003: Improvements to the representation of orography in the Met Office Unified Model. *Quart. J. Roy. Meteor. Soc.*, **129**, 1989–2010.

**Supplemental Material for  
“Thermodynamic bias in the multi-model mean  
boreal summer monsoon”**

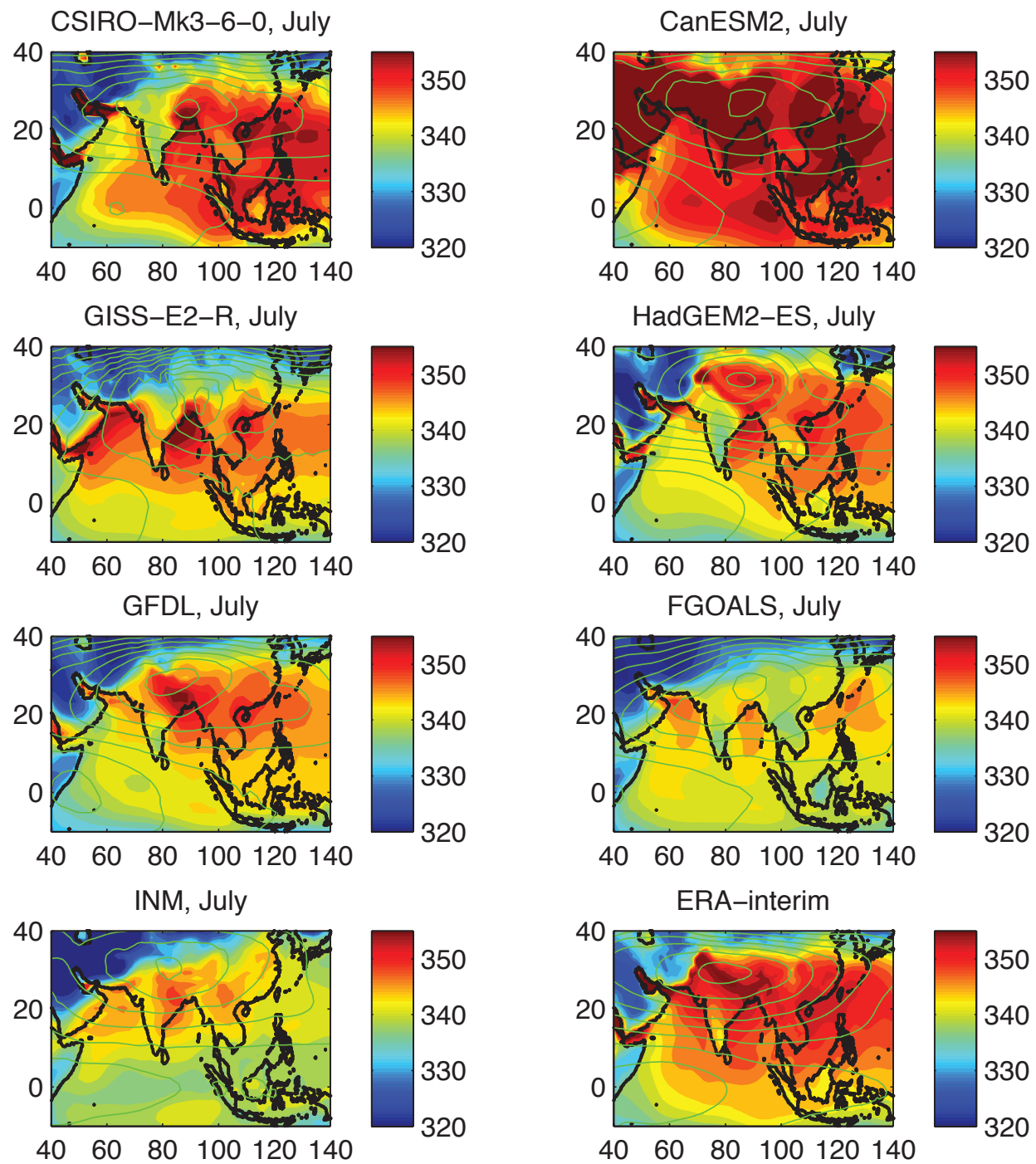
by William R. Boos\* & John V. Hurley

Department of Geology and Geophysics, Yale University  
PO Box 208109, New Haven, CT, USA

\*billboos@alum.mit.edu



**Supplementary Figure 1 | Distributions of  $h_b$  and  $T_u$  for individual CMIP5 models.** July mean surface air moist static energy (shading, in K) and 200-400 hPa temperature (green contours, interval 1 K) for 1979-1999. The ERA-Interim climatology is shown on the next page for comparison.



Supplementary Figure 1 | continued